Liu, Yanling; Zhang, Yanbang; Jia, Guozhi

Article

Photothermal conversion of Bi2Se3 nanosheets and efficient steam generation by capillary siphoning

Energy Reports

Provided in Cooperation with:
Elsevier

Suggested Citation: Liu, Yanling; Zhang, Yanbang; Jia, Guozhi (2020) : Photothermal conversion of Bi2Se3 nanosheets and efficient steam generation by capillary siphoning, Energy Reports, ISSN 2352-4847, Elsevier, Amsterdam, Vol. 6, pp. 1304-1311, https://doi.org/10.1016/j.egyr.2020.05.014

Energy Reports 6 (2020) 1304–1311

Contents lists available at ScienceDirect

Energy Reports

journal homepage: www.elsevier.com/locate/egyr

Research paper

Photothermal conversion of Bi_2Se_3 nanosheets and efficient steam generation by capillary siphoning

Yanling Liu *, Yanbang Zhang, Guozhi Jia *

Tianjin Chengjian University, Tianjin 300384, PR China

ARTICLE INFO

Article history:
Received 28 February 2020
Received in revised form 13 May 2020
Accepted 15 May 2020
Available online xxxx

ABSTRACT

Local heating under light illumination provides a noncontact way to present an enormous superiority for minimum heat dissipation compared with other cases, such as floating on the surface of water. The highly-effective broadband absorption of Bi_2Se_3 covering both infrared and visible wavelength range can result in a high efficiency of 68% at 1 W/cm^2 light illumination. The device possesses the barrier-free path to ensure the generated steam fast escape from the water surface also achieves the local heat generation and straightway wicks the adequate micro-flow to hot zone. The highlighted advantage of our design is that the efficiency is scarcely susceptible even the uninterrupted water flow, unlike the floated film, the heat dissipation is bound to generate due to the heat exchange between the heated and unheated water. The trade-off between temperature and water supplement should be ensured under the large heat generation and maintain an ideal evaporation rate for solar desalinate application.

1. Introduction

Rising demand for freshwater source is becoming increasingly challenging in global for the human's basic survival (Elimelech and Phillip, 2011; Shannon et al., 2008; Koutroulis et al., 2019; Mekonnen and Hoekstra, 2016; Taylor et al., 2014; Degefu et al., 2018). Among the significant solution for freshwater technology, light-to-heat desalination is a prominent pathway based on the clean solar energy and the abundant of sea water on earth (Chandrashekara and Yadav, 2017; Raza et al., 2018a,b; Ambika et al., 2019; Lin et al., 2019a,b; Shan et al., 2019). The investigators have tried their best to realize the steam generation to obtain the freshwater from the seawater using the renewable solar energy. Zhou's group demonstrated the plasmonic absorbers fabricated by self-assembly of aluminum and gold nanoparticles for solar desalination (Zhou et al., 2016a,b,c). Chen's group fabricated a double-layer structure to achieve high temperature by thermal concentration heat localization. Semiconductors were also considered as the effective light-to-heat conversion candidate system to realize the light-to-water evaporation research (Ni et al., 2016). Li Ren's group designed a self-floating MXene Ti_3C_2 thin membrane (Li et al., 2017) and Wu's group developed the Ni-NiO_x/Ni foam for solar thermal water evaporation (Wu et al., 2019). Li Zhuo's group achieved excellent photothermal conversion efficiency by SnSe@SnO_2 core–shell nanocomposite for water evaporation utilizing solar energy (Li et al., 2019). Shan's group fabricated a porous graphene oxide (rGO)/nickel foam structure to realize the harvest of light and the rapid flow of steam, which can converts the absorbed solar energy into heat energy at the water-air interface and can effectively evaporate (Shan et al., 2019). More recently, Shan's group prepared the super-hydrophilic carbonized towel-gourd sponges/paper photothermal layer by the capillarity-driven interfacial self-coating method to improve evaporation rate (Shan et al., 2020). Various studies show that efficiency and cost is the largest obstacle to realize possibility of steam generation industrialization (Fang et al., 2019).

Considering a few fronts, importantly, there are generally a few critical elements for potential applications (Raza et al., 2018a,b; Zhang et al., 2016; Liu et al., 2015; Bae et al., 2015; Zhou et al., 2016a,b,c; Zhang et al., 2015; Tian et al., 2016; Jiang et al., 2016; Liu et al., 2016; Wang et al., 2017a,b; Lin et al., 2019a,b): (i) surface evaporation by heating floating film with or without insulator is one of the significant ways based on the convection properties, by this means, it can achieve the perfect efficiency and minimum heat dissipating to the bulk water. (ii) Floating film can be efficiently wicked the micro-flow to heating zone, thus makes it easier to generate vapor for micro-flow than bulk water. (iii) The selected materials must not only consider the excellent light-to-heat performance, but also the environmental stability due to the severe nature environment and corrosion in potential application (Deng et al., 2014; Birnhack et al., 2008). For above premise critical factors, impressive high-efficiency of evaporation

* Corresponding authors.
E-mail address: jiaguozhi@tcu.edu.cn (G. Jia).

https://doi.org/10.1016/j.egyr.2020.05.014

has been indeed achieved, but the efficiency is bound to undergo a negative impact because heat loss may be generated between heated and unheated water with the flow in practical application. Undoubtedly, noble metal-based thin film is utilized as an optimal light-to-heat converter (Ang et al., 2019; Wang et al., 2016; Skirtach et al., 2005; Zhu et al., 2016, 2018). However, the high-cost, its complex fabrication and inadequate resource restricted its practical application. Bi_2Se_3, one of the novel topological insulator materials, is a promising candidate in many optical and electrical endeavors (Guo et al., 2015, 2013; Peng et al., 2012; Zhang et al., 2011; Yan et al., 2014), especially, its facile fabrication (Min et al., 2012; Lin et al., 2014), abundant resources, as well as excellent photothermal property (originating from the localized resonant surface plasmon) (Jia et al., 2015; Xie et al., 2016; Zhao et al., 2019) making it could be an extraordinarily rational chosen as the photothermal material for water evaporation in practical application.

Herein, we demonstrate a highly-effective Bi_2Se_3-coated capillary tube (Bi-CT) evaporation device. Our device is composed of low-cost Bi_2Se_3 and common glass capillary tube without any insulation, presenting enhanced light-to-heat conversion as well as effective localized heat, especially, noncontact way (the Bi_2Se_3 coating without any contact with water) is more significantly for minimum heat dissipation under light illumination during evaporation process. Combination with the efficient paths for enough water supply and barrier-free steam escape from capillary tube, our design is particularly favorable for effective evaporation. Furthermore, the efficiency is scarcely affected even the water flow continually under the action of natural environment, which provides a crucial guiding significance for the potential application. Besides, based on such-designed evaporation device, evaporation rate and thermal efficiency could be significantly enhanced in comparison with Bi_2Se_3 film under the same light illumination.

2. Results and discussion

A detailed characterization of Transmission electron microscopy (TEM) was performed to elucidate the crystalline structure of the as-grown Bi_2Se_3 nanostructure, as shown in Fig. 1a. The inset (I) of Fig. 1a shows a low magnification bright field TEM image of the Bi_2Se_3 with a folded edge and demonstrates the layer like structure of Bi_2Se_3. A fast Fourier transform (FFT) analysis as depicted by the red box area in Fig. 1(a) verifies high quality crystalline nature of Bi_2Se_3 nanostructure. The expected hexagonal lattice fringes with a lattices pacing of 0.234 nm and 0.31 nm in insert (III), consistent with the spacing of the (1010) planes and (015) of layered Bi_2Se_3, respectively. The existence of Bi and Se in the sample with approximate atomic ratio of 2:3 based on Energy-dispersive X-ray spectroscopy (EDS) analysis (Fig. 1b). Fig. 1c shows the XRD patterns of the as-synthesized powder. All diffraction peaks can be exclusively indexed as rhombohedral structured Bi_2Se_3 phase with lattice constants of a = 0.4139 nm and c = 2.8636 nm and space group of R3m (JCPDS Card No. 33-0214). There were no detectable second phase impurity peaks in the XRD diffractograms. The full width at half maximum (FWHM) of (015) peak suggests that the average crystallite size of the hierarchical Bi_2Se_3 nanostructures to be 319 nm by using the Debye–Scherrer formula. The binding energy of the XPS spectra in Fig. 1d was calibrated based on the carbon C1s peak at 284.6 eV. In the survey spectrum (Fig. 1(d), all of the peaks corresponding to the elements Bi, Se, and C were identified. The presence of a trace amount of C in the spectrum is due to atmospheric carbon, but the gas molecules do not form any chemical bonds with Bi, or Se.

Fig. 2a shows the high concentration Bi_2Se_3 paint by dispersing as-prepared Bi_2Se_3 product into ethanol, where the ethanol is used because of the fast volatilization and solidification for Bi_2Se_3 coating. The Bi-CT was fabricated by brushing Bi_2Se_3 paint onto one end of capillary tube and then immobilization at 150 °C for 3 h. As shown in Fig. 2b, the uniformly Bi_2Se_3 coating is formed and the thickness is easily-controlled through the cycles brushing times. Then the as-fabricated Bi-CT is inserted into the bulk water, and one end of Bi_2Se_3 is exposed in air without any insulation, naturally. The micro-flow quickly climbs up to a certain height in a capillary. Fig. 2c shows the steam generation under the excitation of 808 nm laser, the heating zone of device is not in direct contact with bulk water, instead, the Bi_2Se_3 coating is exposed to the air ensuring much suppressed heat loss to the bulk water. As we seen, the capillary tube wicks micro-flow to the heating zone, the generated heat energy easily transfers to the steam. Simultaneously, efficient water provisions to the heating zone with the escape of the generated vapor in a capillary tube. Therefore, high evaporation rate and thermal efficiency of our device are based on the above-mentioned particular advantages. There is no doubt that the absorption characteristics of nanomaterials in the near-infrared band largely determine the photothermal conversion performance. The absorption spectra of Bi_2Se_3 nanosheets in the band of 200–900 nm are given in Fig. 2d. It can be clearly seen that the nanosheets have good absorption characteristics in the visible and near-infrared band.

The photothermal property of the Bi-CT is investigated under 808 nm near-infrared laser illumination with a density of 2 W/cm^2 (available illumination area is 0.25 cm^2). An infrared thermo detector is used to measure the temperature in air. Under the light irradiation, a steady-state temperature for the Bi_2Se_3 coating could be reached in a short time, which is defined as the temperature when the radiative heat flux is at equilibrium between heat generation and heat dissipation (Zhang et al., 2015). Fig. 3a presents a similar steady-state temperature for varying diameter of Bi-CT under the same light irradiation area. The Bi-CT quickly increases to its steady-state temperature of 82 ± 2 °C while the blank capillary tube presents a steady-state temperature of ≈25.7 °C. It indicates the outstanding photothermal conversion property of Bi_2Se_3 coating. Fig. 3b shows the frequently fluctuated steady-state temperature of Bi-CT, which may originate from the supplementary cold water from the below with the vapor escape during evaporation. The following detailed explanation, for supplementary cold water, it certainly will absorb heat energy before phase changed to steam. The temperature would restore after steam generation. Apparently, Bi-CT-1.0 presents a higher temperature than those (Bi-CT-0.5 and Bi-CT-0.3 shows almost accordance temperature) are less mass change (Fig. 3c) during evaporation. The seemingly unreasonable results can be explained as follows: the corresponding mathematical mode is used to illustrate the water column height in different capillary tube, the formula: $\mathbf{h} = 4\boldsymbol{\gamma cos\theta}/\boldsymbol{\rho g d}$, where h is the water column height, γ and θ are the surface tension and contact angle, respectively. The ρ, g, d are water density, acceleration of gravity and diameter of capillary tube, respectively. According to the formula, the water column height is lower for Bi-CT-1.0 than that for Bi-CT-0.5 and Bi-CT-0.3, as shown in Fig. 4a. Factually, in the case of using Bi-CT-1.0, only a part of laser is irritated into the micro-flow, while another part merely heats the upper air. Therefore, there occur such results that higher temperature but less mass change for Bi-CT-1.0 compared with Bi-CT-0.5 and Bi-CT-0.3.

The mass change over time under light illumination at 2 W/cm^2 is recorded in Fig. 3a. Obviously, the Bi-CT presents high efficient steam generation when it contrasts with blank CT (there is almost no mass change) under light illumination at 2 W/cm^2. Compared with the results of mass change for Bi-CT-0.5 and Bi-CT-0.3, the less mass change for Bi-CT-1.0 (the red diamond in

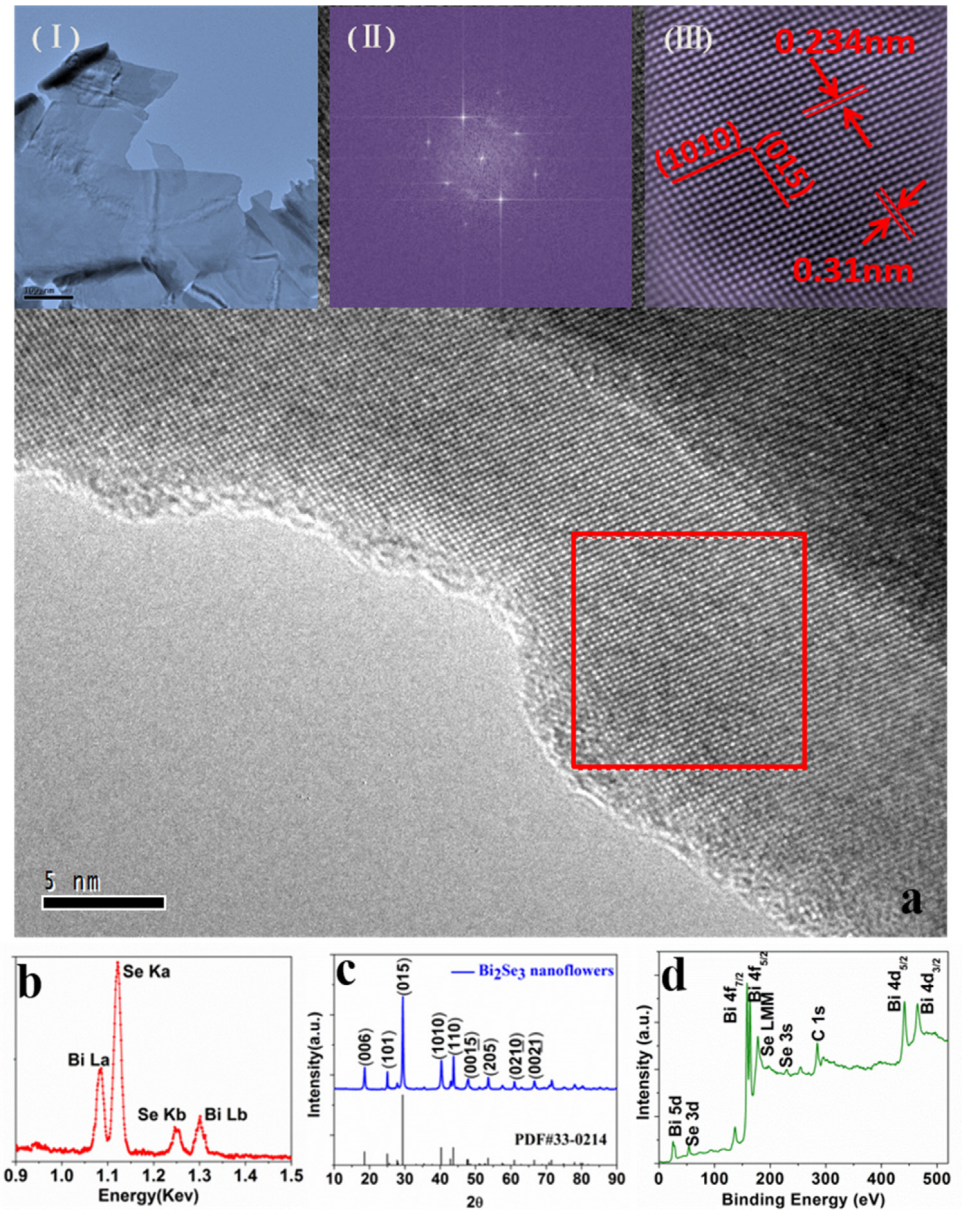

Fig. 1. (a) Magnified TEM image of Bi_2Se_3 nanostructure, showing the highly crystalline nature of the basal plane of Bi_2Se_3 nanostructure. (I) bright field TEM image of typical Bi_2Se_3 nanostructure, (II) corresponding fast Fourier transformation (FFT) pattern (the red box of Fig. 1a). (III) HRTEM image of a Bi_2Se_3 nanostructure, lattice fringes were clearly resolved. (b) Energy-dispersive spectroscopy result of Bi_2Se_3 nanostructure obtained under a TEM. (c) XRD analysis with the black vertical lines being the peaks of Bi_2Se_3 (JCPDS Card No. 33-0214). (d) X-ray photoelectron spectra of the Bi_2Se_3 nanostructure.

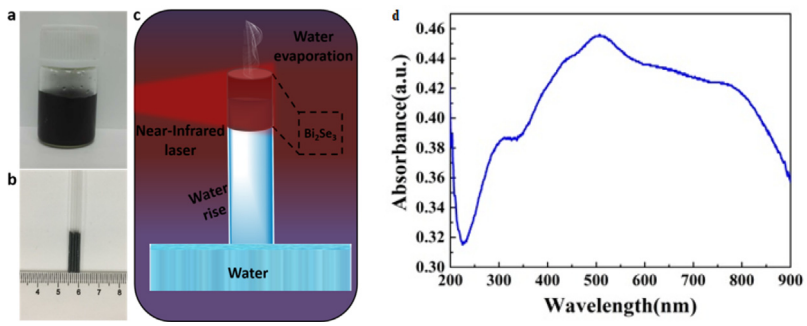

Fig. 2. (a) The high concentration Bi_2Se_3 paint by dispersing the as-prepared Bi_2Se_3 in ethanol. (b) The Bi_2Se_3-coating capillary tube (Bi-CT). (c) The schematic diagram of water column rise in a capillary tube and the evaporation process under laser illumination. (d) The absorption spectrum of Bi_2Se_3 nanosheets in the waveband of 200–900 nm.

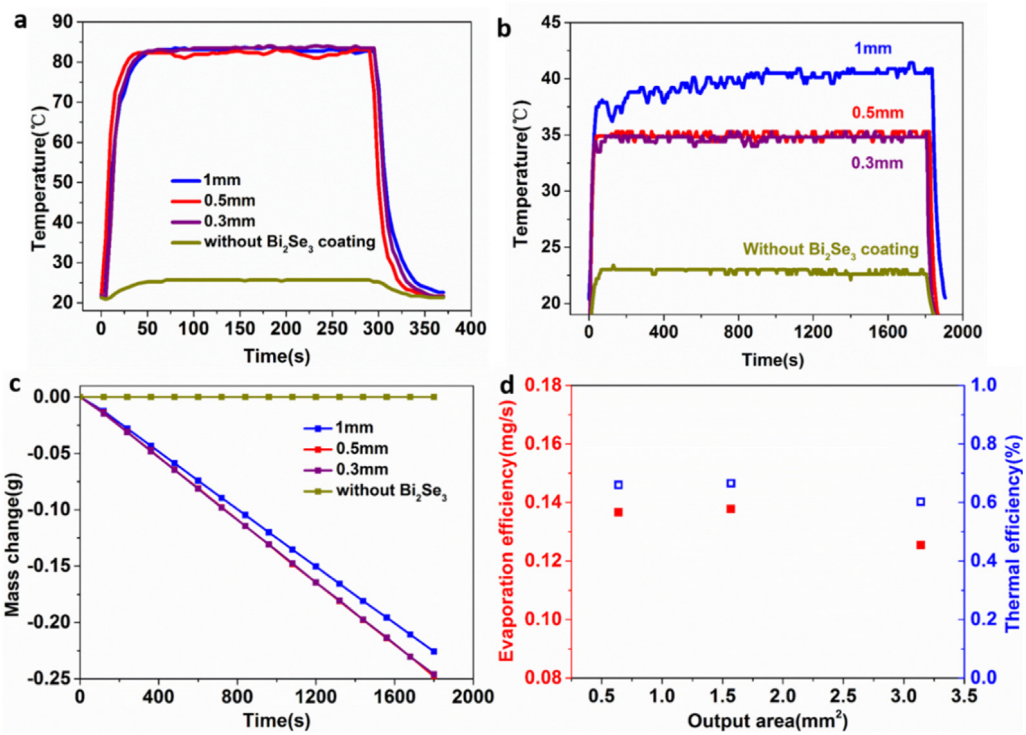

Fig. 3. (a) The temperature profile of varying diameter Bi-CT (0.3, 0.5 and 1.0 mm) and the temperature of bare CT. (b) Temperature changes of Bi-CT over time during evaporation process. (c) Time-dependent of water evaporation performance under various diameter CT. (d) The evaporation rate and thermal efficiency as a function of output area of steam.. (For interpretation of the references to color in this figure legend, the reader is referred to the web version of this article.)

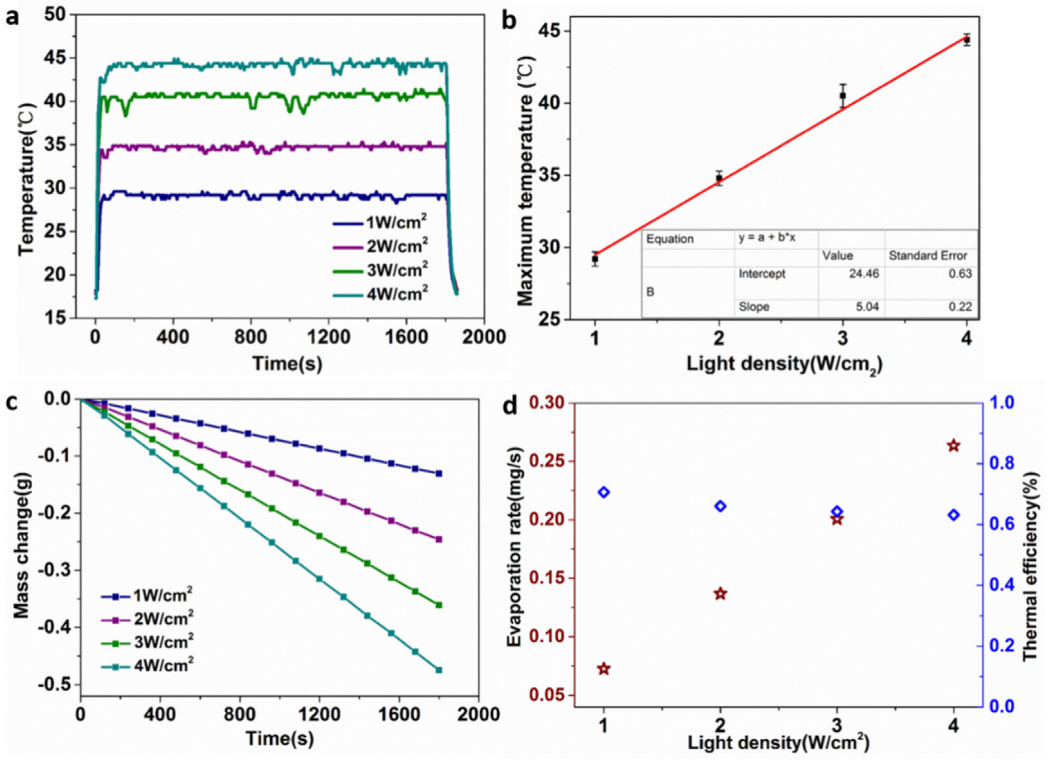

Fig. 4. (a) The temperature profile of Bi-CT-0.3 under various light densities (1, 2, 3 and 4 W/cm^2) in evaporation process. (b) The temperature change of (a), the fitting formula indicating the linearity relationship between (ΔT) and light density. (c) Mass change over time of Bi-CT-0.3 under 1 to 4 W/cm^2 irradiation. (d) The thermal efficiency of the evaporation process by the Bi-CT-0.3 under a range of light density (right-hand side axis) and the corresponding evaporation rate (left-hand side axis).. (For interpretation of the references to color in this figure legend, the reader is referred to the web version of this article.)

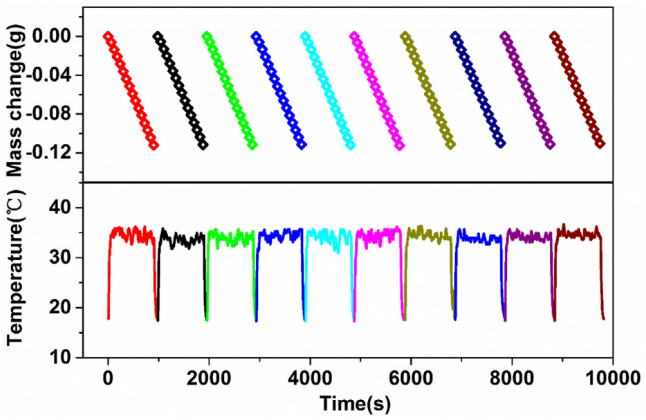

Fig. 5. Evaporation cycle performance of Bi-CT-0.3 over 10 cycles by applying 2 W/cm^2 illumination, with each cycle sustained over 15 min (the corresponding temperature is also shown in figure).

Fig. 3d) demonstrates the small-bore CT is more suitable for evaporation application (such as the evaporation rate of Bi-CT-0.5 and Bi-CT-0.3 reach 0.137 mg/s, while the Bi-CT-1.0 is 0.125 mg/s). The light-to-heat evaporation conversion efficiency (η) (Fig. 3d) of the Bi-CT was calculated by the Zhang's report (Zhang et al., 2015): $\boldsymbol{\eta} = (\boldsymbol{v} \times \boldsymbol{H_e})/\boldsymbol{Q_{laser}}$, where Q_{laser} is the incidence laser density, v is the evaporation rate of water, and H_e is the heat of water evaporation. The conversion efficiency of the Bi-CT-0.3 and Bi-CT-0.5 are then calculated to be ∼66% and ∼66.5 even the output area was only ∼0.64 and ∼1.57 mm^2, respectively, which presents more satisfying result in comparison with the Bi-CT-1.0, whose conversion efficiency is ∼60% (out area is ∼3.14 mm^2).

The selective Bi-CT-0.3 temperature is measured as a function of the time under different incident light density (Fig. 4a). The maximum temperature reach ∼30 and ∼45 °C under light illumination at 1 and 4 W/cm^2, respectively, when 0.66 mm^2 is devoted to evaporation. Furthermore, the maximum temperature is linearly increment in incident light density, as shown in Fig. 4b, where the error bars represent the standard deviation. Fig. 5c shows the mass change as a function of time during vapor generation. These figures show the Bi-CT-0.3 reaches steady-state operation in all evaporation process, demonstrating continuous steam generation under each light density illumination. The evaporation rate increases linearly with increasing light density illumination ascribing to the linear increase in the light density of Bi-CT-0.3 temperature (dark red Pentagram in Fig. 4d). The evaporation rates of Bi-CT-0.3 are ∼0.07 and ∼0.27 mg/s for light intensities of 1 and 4 W/cm^2, respectively. Fig. 4d provides the thermal efficiency of the Bi-CT-0.3 at different incident light density. Thermal efficiency reaches up to ∼68% under laser illumination at 1 W/cm^2, ∼60% under light illumination at 4 W/cm^2, which may be attributed to the enhanced heat dissipate in the air with increasing incident light density.

Durability and stability are also the significant aspects in practical application, which directly reflect the sustainable utilization and insusceptible evaporation performance. Fig. 5 shows the cycle performance of Bi-CT-0.3 under light illumination at 2 W/cm^2. Each cycle is sustained over 15 min without any thermal insulation. It is clearly shown that the mass and temperature changes do not deviate far away from the first plot even for 10 cycles, which are maintained ∼0.12 g and ∼35 °C, respectively.

To illustrate high efficiency of Bi-CT device, the temperature and mass change of Bi_2Se_3 film are recorded under light illumination at 2 W/cm^2 in comparison with CT device, as shown in Fig. 6 a and b. Herein, the Bi_2Se_3 film is fabricated by filter technology. The evaporation device is established as follows: the film is placed on the top of cuvette, not directly contact with bulk water, but the water is supplied using the commercial fiber paper by capillary force. Only one point is touched with Bi_2Se_3 film, wicked the micro-flow to Bi_2Se_3 film along the fiber paper during evaporation process. Note that the mass change is also increased linearly and the temperature is vertically increased to maximum value in a short illumination time (Fig. 6a and b). Based on the measured mass change, maximum mass change of the Bi_2Se_3 thin film (blue) and Bi-CT-0.3 (red) are determined at 1, 2, 3 and 4 W/cm^2 light irradiation, as depicted in Fig. 7a. The mass change for Bi_2Se_3 thin film is less than that in the case of steam generation by using Bi-CT-0.3 device at each light density. For example, the maximum mass change is ∼0.48 g for Bi-CT-0.3, while ∼0.44 g for Bi_2Se_3 film with 4 W/cm^2 illumination. The Bi-CT-0.3 device offers excellent performances for the light-to-heat conversion efficiency and the evaporation rate that compared with thin film device even with the merely output area of ∼0.66 mm^2, as shown in Fig. 7b. These results further demonstrate our designed device is more idealized for exploring a highly efficient and low-cost desalinate system.

This work for Bi-CT has been compared with other works in terms of the efficiency, power density and limitation, as shown in Table 1. A lot of work shows that water evaporation has become an important development direction based on nanotechnology. However, nanomaterials based on practical applications need several important characteristics, such as low cost, high efficiency, and stability. Although the efficiency of the Bi-CT is not the highest, this may provide a new way to avoid the decrease of efficiency caused by ion covering during the process of water evaporation. This may become an important development direction of water treatment technology based on evaporation principle. Although the evaporation rate and efficiency of 68% are lower than the state levels of various evaporation systems, there are several important advantages for the evaporation system. The surface evaporation by heating floating film with or without insulator is one of the significant ways based on the convection properties. By this means it can achieve the perfect efficiency and minimum heat dissipating to the bulk water. The noncontact way is more significant for minimum heat dissipation under light illumination during evaporation process. Combine with the efficient paths for enough water supply and barrier-free steam escaped from capillary tube. Furthermore, the efficiency is scarcely affected even the water flow continually under the action of natural environment, which provides a crucial guiding significance for the potential application.

In conclusion, we have developed a highly-effective capillary tube evaporation device. Our device possesses the barrier-free path to ensure the generated steam fast escape from the water

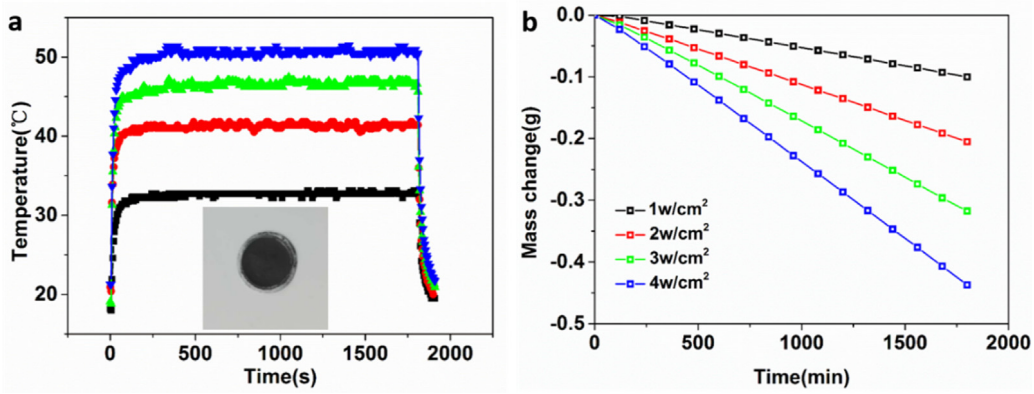

Fig. 6. (a) The time-dependent temperature scheme of the Bi_2Se_3 film in evaporation process, insert shows the formed Bi_2Se_3 film by filter method. (b) Evaporation mass change of Bi_2Se_3 film under a range of incident light density (1, 2, 3 and 4 W/cm^2).

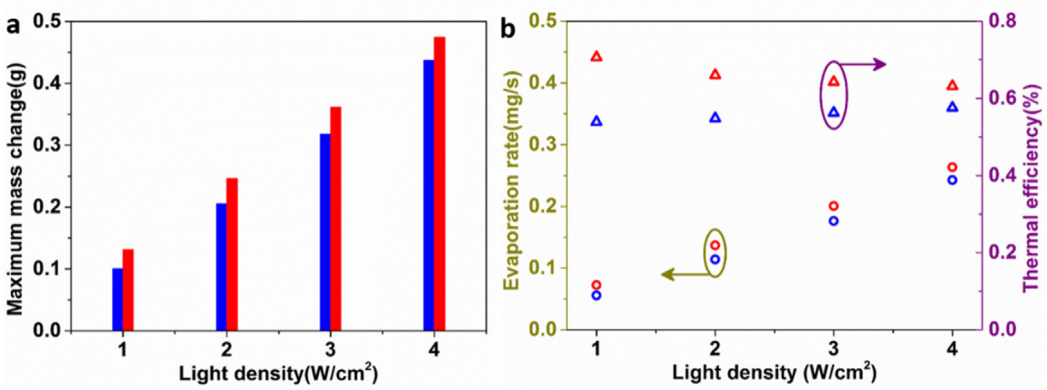

Fig. 7. (a) Comparison scheme of the maximum mass change of the Bi-CT-0.3 and Bi_2Se_3 film under a range of incident light density. (b) The evaporation rate (left-hand side axis) and corresponding thermal efficiency (right-hand side axis) in the evaporation process, red and blue represent the Bi-CT-0.3 and Bi_2Se_3 film, respectively. . (For interpretation of the references to color in this figure legend, the reader is referred to the web version of this article.)

Table 1
The important parameters of Bi-CT comparison with other work.

Ref	Material	Evaporation rate (kg m^{-2} h^{-1}) or efficiency (%)	Power density (sun; 1 sun = 1 kW m^{-2})	Limitation
Lin et al. (2019a)	Cu nanoparticles	2.3256	2	Low efficiency
Shan et al. (2019)	Grapheme oxide/nickel foam	83.4	1	Expensive
Zhou et al. (2016a)	Al nanoparticles	90	6	High power density and Expensive
Zhou et al. (2016c)	Au/NPT	90	4	Expensive
Li et al. (2017)	MXene Ti_3C_2	84	1	No cheap
Wu et al. (2019)	Ni-NiO_x/Ni foam	94	1.41	Poisonous
Li et al. (2019)	SnSe@SnO_2	1.19	1	Low efficiency
Shan et al. (2020)	Carbonized sponges	95.9	1	Energy consumption
Zhang et al. (2016)	Cu_7S_4 nanocrystals	77	1.006	No reusable and Complex
Liu et al. (2016)	Carbon nanotube nanofluid	46.8	1	Energy consumption
Wang et al. (2017b)	Au nanoparticles	65	1	Expensive
Wang et al. (2017a)	Au nanoparticles	85	10	Expensive and high power density
Ang et al. (2019)	Pt-MBT@Ag core–shell NS arrays	98	0.8	Expensive
This work	Bi_2Se_3 nanosheets	68	1	Low cost, no poisonous, reusable

surface. It achieves the local heat generation and straight way wicks the adequate micro-flow to hot zone. More importantly, noncontact way with bulk promote the more-effective steam generation because of the minimum heat dissipate to bulk water, meanwhile, avoid the corrosion for heating Bi_2Se_3 coating. In addition, the efficiency is hardly unaffected even in the flow of bulk water. Our device presents a thermal efficiency of 68% at 1 W/cm^2 light illumination, while generating vapor in open air without any insulation. We believe that there is a trade-off between temperature and water supplement. The proper supplement should be ensured under the large heat generation, thus available achieving a satisfying result concerning reduce heat waste, meanwhile, maintain an ideal evaporation rate. Furthermore, the high-effective broadband absorption of Bi_2Se_3 is whether in infrared or visible light, actually, the amazing efficiency is bound to achieve under the solar illumination. Our work opens a significant approach for solar desalinate for potential application.

3. Experiment sections

3.1. Synthesis of Bi_2Se_3 nanomaterial

The Bi_2Se_3 nanomaterial is synthesized by microwave-assisted method, as follows: 0.3786 g $Bi(NO_3)_3 \cdot {}_5H_2O$, 0.2014 g $NaSeO_3$, 0.4666 g PVP and 0.2495 g NaOH were dissolved in 60 mL ethylene glycol. The homogenized mixture was obtained by magnetic stirring and then heated to 180 °C with a power 300 W for 60 min in a microwave. After reaction, when the mixture was cooled down to room temperature, the precipitate was repeat washed with deionized water and ethanol for three times through centrifugation at 8000 rpm for 20 min, respectively. The final product was collected to further use.

3.2. Characteristics

The microstructure of Bi_2Se_3 were determined by a scanning electron microscopy (SEM, Hitachi S-3500N, 20 kV) and a transmission electron microscopy (TEM, FEI Tecnai G2 S-Twin, 300 kV), equipped for energy dispersive X-ray spectroscopy in the STEM mode. X-ray measurement was performed using a Rigaku-D/MAX-2550PC X-ray diffract meter using Cu Ka Radiation ($\lambda = 0.15418$ nm). Ionic states and composition of the Bi_2Se_3 were analyzed via X-ray photoelectron spectroscopy (XPS) (XPS, PHI 5300) with energy of 1486.6 eV.

3.3. Bi_2Se_3-Coated capillary tube and Bi_2Se_3 film fabrication

All procedures were performed in ambient environment. Above as-prepared Bi_2Se_3 nanostructure was again dispersed in ethanol and then sonication for a few time, forming the high concentration Bi_2Se_3 paint. Next, the Bi_2Se_3 paints was painted on the one end of capillary tube with a common brush. The thickness of capillary tube was 0.5 mm. The thermal conductivity of the tube was 0.00484 Cal/(cm s °C). The process was carried out repeatedly under the hot-blast air until to form the uniform coating on them. Sequentially, the Bi_2Se_3-coated capillary tube (Bi-CT) was further dried on a hot-plates at 150 °C for 60 min and then they were cooled down to room temperature naturally. The Bi_2Se_3 film was fabricated by the filter method, the as-synthesized high concentration Bi_2Se_3 paint was diluted by adding to properly deionized water and 5 ml solution was deposited onto a porous mixed nylon membrane filter (13 mm in diameter, 0.45 μm pore size) to form a Bi_2Se_3 film (∼3 μm), following drying at 60 °C in ambient environment.

3.4. Water evaporation experiment

The evaporation experiments were carried out under a continue wave 808-nm near-infrared laser (MDL-III-808-2W, Changchun New Industries, CNI. China). In our experiment, the water was contained by a cuvette and the Bi-CT placed in the water (one end with Bi_2Se_3 was exposed in the air and Bi_2Se_3 coating was no contact with water, available illumination area was ∼0.25 cm^2, the average thickness of Bi_2Se_3 coating was ∼0.66 μm). For Bi_2Se_3 film evaporation device, a paper-based Bi_2Se_3 film (∼3.36 μm thick) was placed on the surface of fiber paper, another fiber bar was used to supply water by contacting with the fiber paper on the top of cuvette and the other end was soaked in the water. The evaporation temperature was measured by an infrared radiation thermometer (LSCI-SJG300A, Jiangsu, Nanjing Longshu instrument and Meter. China) and was recorded one time per 5 s. The mass change was measured by a high accuracy balance (FA 1004, 0.1 mg in accuracy) and real-time recorded the mass change, then calculating the evaporation rate and efficiency of light steam generation.

CRediT authorship contribution statement

Yanling Liu: Conceptualization, Data curation, Writing - original draft, Writing - review & editing. **Yanbang Zhang:** Data curation, Formal analysis. **Guozhi Jia:** Conceptualization, Data curation, Writing - original draft, Writing - review & editing.

Declaration of competing interest

The authors declare that they have no known competing financial interests or personal relationships that could have appeared to influence the work reported in this paper.

Acknowledgments

We would also like to acknowledge financial supports by the National Natural Science Foundation of China (No. 11674240 and No. 11504261) and the key project of the Natural Science Foundation of Tianjin, China (19JCZDJC38600).

References

Ambika, S., Gopinath, S., Saravanan, K., 2019. Structural, morphological and optical properties and solar cell applications of thioglycolic routed nano cobalt oxide material. Energy Rep. 5, 305–309.
Ang, E.H., Tan, Y.Z., Chew, J.W., 2019. Three-dimensional plasmonic spacer enables highly efficient solar-enhanced membrane distillation of seawater. J. Mater. Chem. A.
Bae, K., et al., 2015. Flexible thin-film black gold membranes with ultrabroadband plasmonic nanofocusing for efficient solar vapour generation. Nat. Commun. 6, 10103.
Birnhack, L., Penn, R., Lahav, O., 2008. Quality criteria for desalinated water and introduction of a novel, cost effective and advantageous post treatment process. Desalination 221, 70–83.
Chandrashekara, M., Yadav, A., 2017. Water desalination system using solar heat: A review. Renew. Sustain. Energy Rev. 67, 1308–1330.
Degefu, D.M., Weijun, H., Zaiyi, L., 2018. Mapping monthly water scarcity in global transboundary basins at country-basin mesh based spatial resolution. Sci. Rep. 8 (1), 2144.
Deng, A., et al., 2014. Impact of pH level and magnesium addition on corrosion of re-mineralized seawater reverse osmosis membrane (SWRO) product water on pipeline materials. Desalination 351, 171–183.
Elimelech, M., Phillip, W.A., 2011. The future of seawater desalination: Energy, technology, and the environment. Science 333, 712–717.
Fang, Q.L., Li, T.T., Chen, Z.M., Lin, H.B., Wang, P., Liu, F., 2019. Full biomass-derived solar stills for robust and stable evaporation to collect clean water from various water-bearing media. ACS. Appl. Mater. Interfaces 11, 10672–10679.
Guo, Y., et al., 2013. Selective-area van der waals epitaxy of topological insulator grid nanostructures for broadband transparent flexible electrodes. Adv. Mater. 25, 5959–5964.
Guo, Y., et al., 2015. 2D hybrid nanostructured Dirac materials for broadband transparent electrodes. Adv. Mater. 27, 4315–4321.
Jia, G.Z., et al., 2015. Excellent photothermal conversion of core/shell cdse/bi$_2$se$_3$quantum dots. Nano. Res. 8, 1443–1453.
Jiang, Q., et al., 2016. Bilayered biofoam for highly efficient solar steam generation. Adv. Mater. 28, 9400–9407.
Koutroulis, A.G., Papadimitriou, L.V., Grillakis, M.G., 2019. Global water availability under high-end climate change: A vulnerability based assessment. Glob. Planet. Change 175, 52–63.
Li, Z., Sun, L., Liu, Y., 2019. Snse@sno$_2$ core–shell nanocomposite for synchronous photothermal–photocatalytic production of clean water. Environ. Sci.-Nano 6 (5), 1–3.
Li, R., Zhang, L., Shi, L., Wang, P., 2017. MXene Ti_3C_2: An effective 2D light-to-heat conversion material. Acs. Nano 11 (4), 3752–3759.
Lin, Y., Chen, Z., Fang, L., 2019a. Copper nanoparticles with near-unity, omnidirectional, and broadband optical absorption for highly efficient solar steam generation. Nanotechnology 30 (1), 015402.
Lin, Y., Xu, H., Shan, X., Di, Y., Zhao, A., Hu, Y., 2019b. Solar steam generation based on photothermal effect: From designs to applications, and beyond. J. Mater. Chem. A 7 (33), 19203–19227.
Lin, Z., et al., 2014. Solution processable colloidal nanoplates as building blocks for high-performance electronic thin films on flexible substrates. Nano. Lett. 14, 6547–6553.
Liu, Y., et al., 2015. A bioinspired, reusable, paper-based system for high-performance large-scale evaporation. Adv. Mater. 27, 2768.

Liu, X., et al., 2016. Direct vapor generation through localized solar heating via carbon nanotube nanofluid. Energ. Convers. Manage..
Mekonnen, M.M., Hoekstra, A.Y., 2016. Four billion people facing severe water scarcity. Sci. Adv. 2, e1500323.
Min, Y., et al., 2012. Quick, controlled synthesis of ultrathin bi_2se_3 nanodiscs and nanosheets. J. Am. Chem. Soc. 134, 2872–2875.
Ni, G., Li, G., Boriskina, S.V., Li, H., 2016. Steam generation under one sun enabled by a floating structure with thermal concentration. Nat. Energy 1 (9), 16126.
Peng, H., et al., 2012. Topological insulator nanostructures for near-infrared transparent flexible electrodes. Nature Chem. 4, 281–286.
Raza, A., Lu, J.Y., Alzaim, S., 2018a. Novel receiver-enhanced solar vapor generation: Review and perspectives. Energies 11, 253.
Raza, A., Lu, J.Y., Alzaim, S., Zhang, T.J., 2018b. Novel receiver-enhanced solar vapor generation:review and perspectives. Energies 11, 253.
Shan, X., Lin, Y., Zhao, A., 2019. Porous reduced graphene oxide/nickel foam for highly efficient solar steam generation. Nanotechnology 30 (42), 425403.
Shan, S., Zhao, A.Q., Y.W., Lin., Y.J., Hu., 2020. Low-cost, scalable, and reusable photothermal layers for highly efficient solar steam generation and versatile energy conversion. Adv. Sustain. Syst. 1900153.
Shannon, M.A., et al., 2008. Science and technology for water purification in the coming decades. Nature 452, 301–310.
Skirtach, A.G., et al., 2005. The role of metal nanoparticles in remote release of encapsulated materials. Nano. Lett. 5, 1371–1377.
Taylor, R., et al., 2014. HYDROLOGY when wells run dry. Nature 516, 179–180.
Tian, L., et al., 2016. Plasmonic biofoam: A versatile optically active material. Nano. Lett. 16, 609–616.
Wang, L., Gutierrez-Cuevas, K.G., Urbas, A., Li, Q., 2016. Near-infrared light-directed handedness inversion in plasmonic nanorod-embedded helical superstructure. Adv. Opt. Mater. 4, 247–251.
Wang, X., He, Y., Liu, X., Zhu, J., 2017b. Investigation of photothermal heating enabled by plasmonic nanofluids for direct solar steam generation. Sol. Energy 157, 35–46.
Wang, X., Y., He., Liu, X., 2017a. Solar steam generation through bio-inspired interface heating of broadband-absorbing plasmonic membranes. Appl. Energy 195, 414–425.
Wu, D., Qu, D., Jiang, W., 2019. Self-floating nanostructural ni-niox/ni foam for solar thermal water evaporation. J. Mater. Chem. A.
Xie, H., et al., 2016. Metabolizable ultrathin bi_2se_3 nanosheets in imaging-guided photothermal therapy. Small 12, 4136–4145.
Yan, Y., et al., 2014. Topological surface state enhanced photothermoelectric effect in bi_2se_3 nanoribbons. Nano. Lett. 14, 4389–4394.
Zhang, L., Tang, B., Wu, J., Li, R., Wang, P., 2015. Hydrophobic light-to-heat conversion membranes with self-healing ability for interfacial solar heating. Adv. Mater. 27, 4889–4894.
Zhang, J., et al., 2011. Raman Spectroscopy of few-quintuple layer topological insulator bi_2se_3 nanoplatelets. Nano. Lett. 11, 2407–2414.
Zhang, C., et al., 2016. Shape-controlled synthesis of high-quality cu_7s_4 nanocrystals for efficient light-induced water evaporation. Small 12, 5320–5328.
Zhao, Z.J., Jia, G.Z., Liu, Y.L., Zhang, Q.R., Zhou, Y.Y., 2019. In-situ synthesized and pattern ag/bi_2se_3 composite structure by LDW and photothermal conversion. Sci. Rep. 9, 1781.
Zhou, L., et al., 2016a. 3D self-assembly of aluminium nanoparticles for plasmon-enhanced solar desalination. Nat. Photonics 10.
Zhou, J., et al., 2016b. Macroscopic and mechanically robust hollow Carbon spheres with superior oil adsorption and light-to-heat evaporation properties. Adv. Funct. Mater. 26, 5368–5375.
Zhou, L., et al., 2016c. Self-assembly of highly efficient, broadband plasmonic absorbers for solar steam generation. Sci. Adv. 2, e1501227.
Zhu, M.W., Li, Y.J., Chen, F.J., Zhu, X.Y., Dai, J.Q., Li, Y.F., Yang, Z., Yan, X.J., Song, J.W., Wang, Y.B., Hitz, E., Luo, W., Lu, M.H., Yang, B.L., Hu, B., 2018. Plasmonic wood for high-efficiency solar steam generation. Adv. Energy. Mater. 8, 1701028.
Zhu, H., Yi, F., Cubukcu, E., 2016. Plasmonic metamaterial absorber for broadband manipulation of mechanical resonances. Nat. Photonics 10, 709–714.